



**Highly stable and isomorphous donor–acceptor stacking in a family of n-type organic semiconductors of BTBT-TCNQ derivatives**

Journal:	<i>Journal of Materials Chemistry C</i>
Manuscript ID	TC-ART-08-2022-003634.R1
Article Type:	Paper
Date Submitted by the Author:	25-Sep-2022
Complete List of Authors:	Matsuoka, Satoshi; Nagasaki University; The University of Tokyo Ogawa, Kazuma; The University of Tokyo Ono, Ryota; The University of Tokyo Nikaido, Kiyoshi; The University of Tokyo Inoue, Satoru; The University of Tokyo, Higashino, Toshiki; National Institute of Advanced Industrial Science and Technology (AIST), Tanaka, Mutsuo; Saitama Institute of Technology Tsutsumi, Junya; National Institute of Advanced Industrial Science and Technology, Flexible Electronics Research Center Kondo, Ryusuke; Okayama University Kumai, Reiji; High Energy Accelerator Research Organization (KEK) , Institute of Materials Structure Science Tsuzuki, Seiji; The University of Tokyo, Applied Physics; Yokohama National University, Institute of Advanced Sciences Arai, Shunto; The University of Tokyo, Applied Physics Hasegawa, Tatsuo; The University of Tokyo, Dept Appl Phys

## ARTICLE

## Highly stable and isomorphous donor–acceptor stacking in a family of *n*-type organic semiconductors of BTBT-TCNQ derivatives

Received 00th January 20xx,  
Accepted 00th January 20xx

Satoshi Matsuoka,<sup>\*a,b</sup> Kazuma Ogawa,<sup>a</sup> Ryota Ono,<sup>a</sup> Kiyoshi Nikaido,<sup>a</sup> Satoru Inoue,<sup>a</sup> Toshiki Higashino,<sup>c</sup> Mutsuo Tanaka,<sup>d</sup> Jun'ya Tsutsumi,<sup>c</sup> Ryusuke Kondo,<sup>e</sup> Reiji Kumai,<sup>f</sup> Seiji Tsuzuki,<sup>a</sup> Shunto Arai<sup>a</sup> and Tatsuo Hasegawa<sup>\*a</sup>

DOI: 10.1039/x0xx00000x

Herein, we present the common structural features of a family of semiconducting molecular donor–acceptor (DA) compounds based on alkylated fused-ring thieno-acenes. Crystal structure analyses were conducted for 22 DA compounds of variously substituted benzothieno[3,2-*b*][1]benzothiophenes (BTBTs), unsubstituted dithieno[3,2-*b*:2',3'-*d*]thiophene, and unsubstituted benzo[1,2-*b*:4,5-*b'*]dithiophene as donors, which were combined with 7,7,8,8-tetracyanoquinodimethane (TCNQ) and its fluorinated derivatives ( $F_m$ TCNQ,  $m = 0, 1, 2, 4$ ) as acceptors. Fourteen DA compounds of (substituted BTBT)(TCNQ derivative) formed isomorphous layered molecular packing, where the intermolecular stacking arrangements between the planar skeletons of BTBT and TCNQ were common to each other, and the various substituents played supplementary roles. Density functional theory calculations were conducted to investigate the intermolecular forces between  $\pi$ -electron cores along the DA stacks. Dispersion interactions were the dominant intermolecular attraction, showing weak stacking position dependence, while the short-range orbit–orbit interaction was always repulsive, irrespective of stacking. An important finding is that the orbit–orbit interaction has a relatively strong position dependence and leads to common structural features in the DA compounds. We discuss the origin of the isostructural nature of molecular DA compounds, which is crucial in searching for and exploring unique combinations of molecules with superior semiconducting characteristics.

### 1. Introduction

A combination of electron donor and acceptor molecules provides a vast variety of electronically functional materials. An example of this combination is (tetrathiafulvalene; TTF)(7,7,8,8-tetracyanoquinodimethane; TCNQ), also known as “organic metal”, which shows very high electrical conductivity.<sup>1–5</sup> Another example is (TTF)(chloranil; CA), also known as “exotic organic semiconductor” (OSC), which exhibits valence instability between the donor and acceptor units.<sup>5–8</sup> Recently, some molecular donor–acceptor (DA) compounds were reported to afford excellent semiconducting characteristics useful for electronic device applications.<sup>9–13</sup> Organic thin-film transistors (TFTs) were obtained with the molecular DA compounds of (dialkylated benzothieno[3,2-*b*][1]benzothiophenes; BTBT)( $F_m$ TCNQ), showing *n*-type operations with a mobility of

approximately  $0.6 \text{ cm}^2\text{V}^{-1}\text{s}^{-1}$ .<sup>14</sup> A high stability of *n*-type characteristics in air was achieved in the devices, which is a required feature in the development of organic complementary circuits and is not feasible in single-component OSCs.<sup>15,16</sup> Additionally, the DA compound films can be fabricated using a simple blade-coating technique, which makes the materials quite promising for applications in printed electronics.

The current research target for manufacturing organic TFTs is mainly focused on single-component OSCs. Among them, alkylated BTBTs have been shown to provide several single-component OSCs that exhibit excellent *p*-type TFT characteristics with intrinsic mobilities higher than  $10 \text{ cm}^2\text{V}^{-1}\text{s}^{-1}$ .<sup>17–21</sup> The formation of the layered herringbone (LHB) packing of the  $\pi$ -electron cores is important for achieving efficient two-dimensional electron transport characteristics. Based on a systematic study of variously substituted BTBTs, the intermolecular packing between  $\pi$ -electron cores was demonstrated to be largely controlled by substituents such as long alkyl chains or phenyl rings.<sup>22–25</sup> The dispersion corrected DFT calculations, which use carefully selected functional and dispersion correction method to reproduce the intermolecular interaction energies of aromatic molecules obtained by CCSD(T) level calculations near saturation, revealed that the layered crystallinity is clearly enhanced by the substituted alkyl chains.<sup>24,26</sup> However, these effects have not yet been demonstrated for other molecular systems, such as two-component DA compounds. Qualitative quantum chemical analyses suggest that charge-transfer (CT) interaction should be crucial for DA compounds.<sup>27</sup> In contrast, the CT mechanism has not yet been demonstrated in first-principle (or *ab*

<sup>a</sup> Department of Applied Physics, The University of Tokyo, Tokyo 113-8656, Japan

<sup>b</sup> Graduate School of Engineering, Nagasaki University, Nagasaki 852-8521, Japan

<sup>c</sup> Research Institute for Advanced Electronics and Photonics (RIAEP), National Institute of Advanced Industrial Science and Technology (AIST), Tsukuba, Ibaraki 305-8565

<sup>d</sup> Department of Life Science & Green chemistry, Saitama Institute of Technology, Fukaya, Saitama 369-0293, Japan

<sup>e</sup> Department of Physics, Okayama University, Okayama 700-8530, Japan

<sup>f</sup> Photon Factory, Institute of Materials Structure Science, High Energy Accelerator Research Organization (KEK), Tsukuba, Ibaraki 305-0802, Japan

† Electronic Supplementary Information (ESI) available: Material syntheses, intermolecular potential calculation of the other molecules, list of DA compounds, bending angle of alkyl chains, electrostatic potentials, cyclic voltammograms, polarized absorption spectra, a transfer curve and TG-DTA measurements. CCDC 2164767-2164788. See DOI: 10.1039/x0xx00000x

initio) quantitative quantum chemical analyses for intermolecular interactions. Thus, the design, selection, and modification of the donor and acceptor units to search for and explore excellent OSCs are still unclear.

In this study, we developed several molecular-compound OSCs comprising variously alkylated BTBTs and related molecules, with combinations of TCNQ and its fluorinated derivatives ( $F_m$ TCNQ with  $m = 0, 1, 2, 4$ ; for short, F0, F1, F2, and F4, respectively).<sup>28–30</sup> Based on crystal structure analyses, we found that most of the DA compounds form isomorphous layered molecular packing, where the intermolecular stacking arrangements between planar donor and acceptor cores are common to each other, irrespective of the type of substituent. To clarify the origin of these structural characteristics, we conducted the dispersion corrected density functional theory (DFT) calculations of the intermolecular forces of the DA compounds. We then investigated the origin of the isostructural DA stacking characteristics in a family of molecular-compound OSCs.

## 2. Experimental

### 2.1 Fabrication of DA compound crystals and thin films

The single crystals of the molecular compounds were prepared by recrystallization via the slow cooling of the saturated solution at 80 °C with acetonitrile as the solvent. The molar ratio of the donor and acceptor units in the solution is different because of the various solubilities that depend on the skeleton and/or substituent group. The thin films of the molecular compounds were fabricated using a blade-coating technique for mixed solutions of donor and acceptor units with a 1:1 molar ratio in chlorobenzene at a concentration of approximately 1.11 gL<sup>-1</sup>. As substrates, we utilized a *p*-doped Si/SiO<sub>2</sub> (100 nm) wafer surface coated with parylene C films (40–75 nm) for improved surface wettability.

### 2.2 Crystal structure analyses

The crystal structures of the DA compounds were analysed using single-crystal X-ray diffraction. LithoLoops were used to mount the crystals for the diffraction measurements. Most of the crystal structure analyses were successfully conducted using a Rigaku AFC10 four-circle diffractometer equipped with a Pilatus 200 K hybrid pixel detector. The structural analyses for (PhC12)(F4) and (PEC12)(F4) were not feasible and were thus conducted using synchrotron radiation with a monochromatized X-ray beam at a photon energy of 12.4 keV at beamline BL-8A of the Photon Factory (PF) in KEK. Bragg reflections were detected using a cylindrical imaging plate diffractometer (IP-DSC, Rigaku). Data correction and reduction were conducted using CrysAlisPro or RapidAuto software. Refinements for all DA compounds were conducted using CrystalStructure<sup>31</sup> and Olex2<sup>32</sup> software packages. In the analyses, all non-hydrogen atoms were refined anisotropically, while hydrogen atoms were refined using the riding model with SHELXL.<sup>33</sup>

### 2.3 Optical and electrical measurements

Polarized optical absorption measurements were conducted using homemade apparatus comprising a monochromator, a halogen

lamp, polarizers, and a two-dimensional CMOS image sensor. The absorbance was analysed by extracting the signal intensity from optical images captured at different wavelengths and polarizer angles. We produced both single-crystal field-effect transistors (FETs) and polycrystalline TFTs for these DA compounds. The former was fabricated by attaching single crystals grown by recrystallization, on a TFT substrate with Cytop gate dielectric layer (400 nm) in a bottom-gate, bottom-contact (BC) geometry with Cr (0.5 nm) / Au (30 nm). The latter was fabricated using a blade-coated semiconductor layer with a top-contact (TC) geometry with Au (30 nm). The crystallographic axes in FET channel were aligned approximately along the stacking axes of the DA compound crystals. The field-effect mobilities were measured using a semiconductor parametric analyser (E5270A, Agilent Technologies Inc.).

### 2.4 Cyclic voltammetry measurements

Cyclic voltammograms were recorded using a potentiostat (Ivium Compactstat, IVIUM Technologies) with a standard three-electrode setup with glassy carbon, platinum wire, and saturated calomel electrode as the working, counter, and reference electrodes, respectively. The measurements were conducted in a degassed and dehydrated benzonitrile solution containing 0.1 M tetra-*n*-butylammonium perchlorate (*n*-Bu<sub>4</sub>N-ClO<sub>4</sub>) at a scan rate of 100 mV s<sup>-1</sup>.

### 2.5 Computational methods

The calculations of the intermolecular energy were conducted using the Gaussian 16 program package.<sup>34</sup> The total intermolecular interaction energy ( $E_{\text{int}}$ ) was calculated by dispersion corrected DFT calculations (B3LYP/6-311G\*\* level<sup>35</sup> with Grimme's D3 dispersion correction<sup>36</sup>). The basis set superposition error (BSSE)<sup>37</sup> was corrected using the counterpoise method.<sup>38</sup> The combination of the B3LYP functional and D3 correction was selected owing to its very good performance in calculating the intermolecular forces of benzene and thiophene.<sup>39</sup> The potentials calculated for the benzene and thiophene dimers using the dispersion corrected DFT calculations are close to the estimated CCSD(T) (coupled cluster calculations with single and double substitutions with non-iterative triple excitations)<sup>40,41</sup> level potentials at the basis set limit. In addition, we have compared the calculated potentials for the thiophene-tetracyanoethylene complex using the dispersion corrected DFT calculations with the CCSD(T) level potential to confirm the accuracy of the dispersion corrected DFT calculations for calculating the intermolecular interaction energies in the donor–acceptor complex. The potential obtained by the dispersion corrected DFT calculations is close to the CCSD(T) level potential at the basis set limit as shown in Fig. S1 in Supplementary Information. The details of the CCSD(T) calculations of the thiophene-tetracyanoethylene complex are shown in supplementary Information.

The contributions of various intermolecular forces were evaluated. The contributions of the electrostatic and induction interactions were calculated from charge distributions of molecules

DA compound		Space group	$a$ (Å)	$b$ (Å)	$c$ (Å)	$\alpha$ (°)	$\beta$ (°)	$\gamma$ (°)	Layer structure
Donor	Acceptor								
<i>monoC12</i>	F0	$P\bar{1}$	7.1729(4)	7.7021(3)	31.1946(14)	93.873(3)	90.246(4)	106.107(4)	Bilayer
	F4	$P\bar{1}$	7.0951(4)	8.1723(4)	30.9664(17)	95.640(4)	92.233(4)	107.801(5)	Bilayer
	F0	$P\bar{1}$	8.7328(3)	13.8481(3)	20.6953(7)	98.214(3)	95.683(3)	99.591(3)	Other 1
<i>EtC8</i>	F2	$P\bar{1}$	7.1298(9)	7.8602(12)	15.388(2)	99.352(13)	95.978(11)	106.494(12)	Disorder
	F4	$P\bar{1}$	7.0402(7)	8.0595(8)	15.2240(13)	99.376(8)	95.115(8)	107.186(9)	Disorder
	F0	$P\bar{1}$	7.2006(9)	7.7712(10)	16.275(2)	83.298(11)	88.753(11)	73.593(11)	Disorder
<i>nBuC8</i>	F2	$P\bar{1}$	7.1024(10)	7.8510(10)	16.023(3)	83.594(13)	88.136(13)	72.994(12)	Disorder
	F4	$P\bar{1}$	7.0441(6)	8.0788(7)	15.9191(14)	84.206(7)	87.707(7)	72.303(8)	Disorder
<i>PhC12</i>	F4	$P\bar{1}$	7.1488(5)	8.1513(6)	34.312(2)	89.7347(13)	84.2336(18)	72.055(2)	Bilayer
<i>PEC12</i>	F4	$P\bar{1}$	7.1644	8.1007	36.0410	89.5940	86.6300	72.4940	Bilayer
	F0	$P2_1$	7.1741(4)	68.852(3)	7.6437(4)	90	104.296(5)	90	Bilayer (Chiral)
	F2	$P\bar{1}$	7.2476(2)	7.7466(2)	34.0492(9)	90.329(2)	91.785(2)	105.902(2)	Bilayer
<i>oTolC10</i>	F4	$P\bar{1}$	7.1776(2)	7.9582(2)	33.8312(9)	90.385(2)	91.878(2)	106.112(3)	Bilayer
	F0	$P\bar{1}$	7.6951(3)	8.7806(3)	28.7331(11)	95.671(3)	92.392(3)	111.895(3)	Other 2
	F2	$P\bar{1}$	7.17641(19)	7.8969(2)	34.0663(8)	83.678(2)	84.332(2)	72.824(2)	Bilayer
<i>mTolC10</i>	F4	$P\bar{1}$	7.1222(6)	8.1373(7)	33.804(2)	96.586(6)	91.082(6)	107.646(8)	Bilayer

**Table 1** Unit cell parameters for (unsymmetric substituted BTBTs)( $F_m$ TCNQ) compounds.

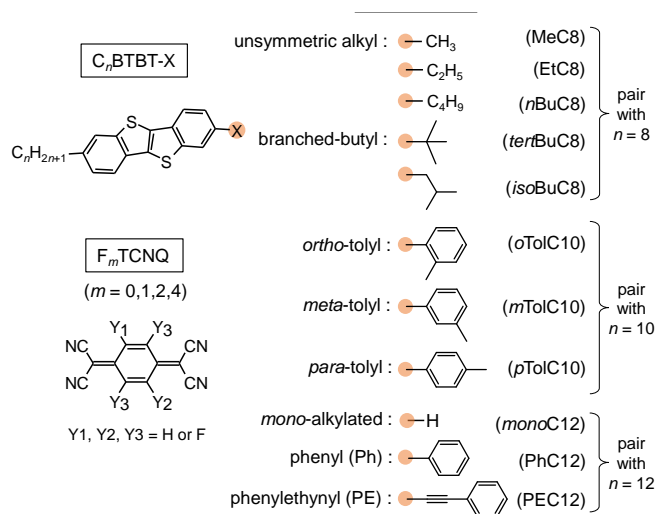


**Fig. 1** Molecular structure of the donor and acceptor units.

obtained by the DFT calculations and atomic polarizabilities. The contributions of the dispersion interactions were evaluated as the difference between the interaction energies calculated with and without the dispersion correction, since the DFT calculations using the B3LYP functional cannot evaluate the dispersion interactions. The interaction energies obtained by DFT calculations using the B3LYP functional include the contributions of the orbit-orbit (CT and exchange-repulsion), electrostatic and induction interactions.

The electrostatic ( $E_{es}$ ) and induction ( $E_{ind}$ ) energies were calculated using ORIENT version 3.2.<sup>42</sup> The electrostatic energy of the

complex was calculated as interactions between the distributed multipoles of molecules. Distributed multipoles<sup>43,44</sup> up to hexadecapole on all atoms were obtained using the B3LYP/6-311G\*\* wave functions of an isolated molecule with the GDMA program.<sup>45</sup> The induction energy was calculated as interactions of polarizable sites with the electric field produced by the distributed multipoles of monomers.<sup>46</sup> The atomic polarizabilities of carbon ( $\alpha = 10$  au), nitrogen ( $\alpha = 8$  au), and sulphur ( $\alpha = 20$  au) were used for the calculations.<sup>47</sup> Distributed multipoles were used only to estimate the electrostatic and induction energies. The interaction energy calculated without dispersion correction ( $E_{b3lyp}$ ) is approximately the sum of the electrostatic, induction, and short-range (orbital-orbital) interaction energies ( $E_{short}$ ).  $E_{short}$  was calculated according to the equation  $E_{short} = E_{b3lyp} - E_{es} - E_{ind}$ . The dispersion energy ( $E_{disp}$ ) was calculated as the difference between the calculated interaction energies with and without dispersion correction according to the equation  $E_{disp} = E_{int} - E_{b3lyp}$ .

### 3. Results and discussion

#### 3.1 Crystal structure of (substituted BTBT)( $F_m$ TCNQ) [ $m = 0, 1, 2, 4$ ]

We used 11 types of unsymmetrically substituted BTBT and four types of  $F_m$ TCNQ as the donor and acceptor units, respectively, as shown in Fig. 1. All of donor molecules were synthesized according to reported procedures of BTBT derivatives with several modifications, as described in Supporting Information. We observed complex formations for all combinations through the colour change

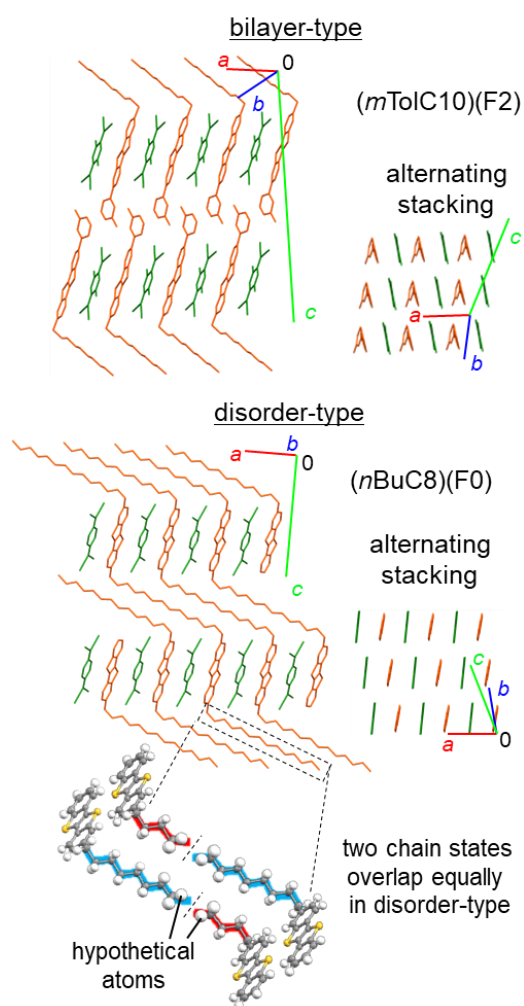


**Fig. 2** Typical crystal structure of bilayer- and disorder-type DA compounds. In-plane structures are drawn without alkyl chains. Donor and acceptor molecules are coloured orange and green, respectively. Gray, white, and yellow atoms are carbon, hydrogen, and sulphur, respectively.

of solutions, which is attributable to the hybridization of molecular orbital levels between the donor and acceptor units. The results of the crystallization and structural analyses for all combinations are summarized in Supplementary Table S1. Recrystallized products from the solutions were not obtained for several combinations. Furthermore, conducting crystal structure analysis on recrystallized products for some combinations was not possible because they were fibre-like and excessively thin to measure, as shown in Supplementary Fig. S2.

We successfully analysed the crystal structures of 16 DA compounds for (substituted BTBT)( $F_m$ TCNQ) [ $m = 0, 1, 2, 4$ ], the results of which are summarized in Table 1. We found that all obtained structures comprised alternating  $\pi$ -stacking, where the planar  $\pi$  electron cores of the donor and acceptor units face each other. These core–core and eventual inter-stack arrangements form a layered packing, where the  $\pi$ -conjugated semiconducting layers are separated by an alkyl-substituent layer, showing layered crystalline characteristics. We found that 14 DA compounds form a stacking structure quite similar to that of (dialkylated

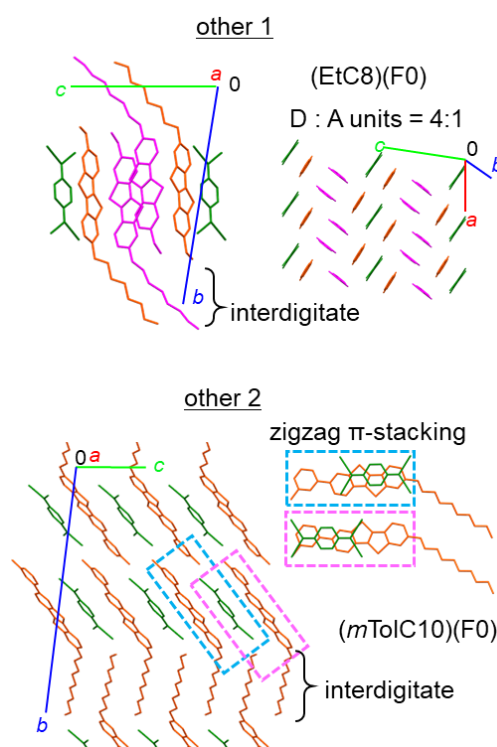


**Fig. 3** Crystal structures of two exceptions: (EtC8)(F0) (other 1) and (*mTolC10*)(F0) (other 2). Alternating stacking donor and acceptor units are coloured orange and green, respectively. Paired donor molecules are coloured pink.

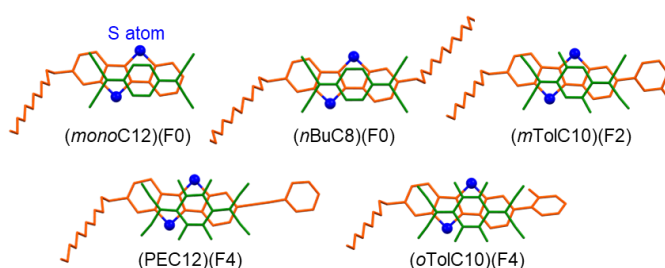


**Fig. 4** Intermolecular arrangements of five DA compounds along the alternating stacking axis. Sulphur atoms are represented by blue-filled circles.

BTBT)( $F_m$ TCNQ).<sup>10</sup> The other two DA compounds form different types of crystal structures, which will be described later. The former structure can be categorized into two types in terms of the long-axis orientation of unsymmetrically substituted BTBT (as shown in Fig. 2): bilayer and disorder. The bilayer type comprises unipolarly oriented unsymmetric molecules, with the respective layers forming an alternating antiparallel alignment such that the alkyl substituents (and counter substituents) are in tail-to-tail (head-to-head) contact. Among them, (*oTolC10*)(F0) retains chirality exclusively in its bilayer-type structure. The disorder-type involves disorder of long-axis orientations for unsymmetric BTBT molecules, which emerges only when the BTBT core is substituted unsymmetrically by two alkyl substituents of different lengths. Nonetheless, the total thickness of the substituent layer was maintained at a chain length because the

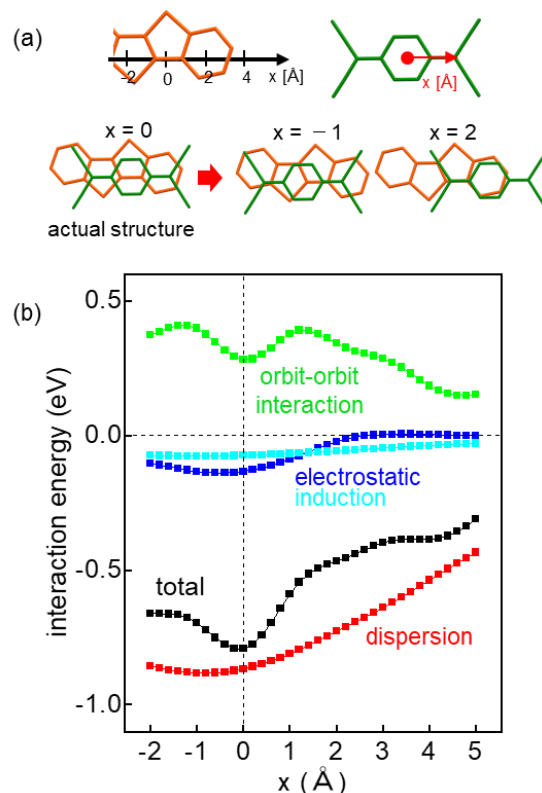
tail-to-tail contact of alkyl chains is always formed by a combination of alkyl chains with different lengths. Interestingly, the structure analysis indicates that the interlayer alkyl chains seem to be continuous between adjacent BTBT cores, where two hypothetical carbon atoms are assumed to connect the ends of the alkyl chains instead of contacting the terminal hydrogen atoms.

Fig. 3 presents the crystal structures of two exceptions to the above observation: (EtC8)(F0) and (*m*TolC10)(F0), named as other 1 and other 2, respectively. Other 1 is formed by a combination of donor and acceptor at a molar ratio of 4:1 and comprises two types of units whose short axis orientations are orthogonal to each other. The first unit comprises paired donor molecules, while the other unit comprises two donors and one acceptor, which are stacked in an alternating arrangement. Other 2 seems to be similar to the bilayer type; however, the alternating stacking arrangement is different: all overlaps between the donor and acceptor units are not equivalent. Half of the overlaps are shifted to the substituent (i.e., *m*Tol moiety) side of the donor molecule along the molecular long axis, forming zigzag  $\pi$ -stacking. Additionally, the alkyl chains in both DA compounds (other 1 and other 2) are interdigitated with each other between the adjacent layers.<sup>48–50</sup> Note that such unique structures are only obtained when non-fluorinated TCNQ is utilized as an acceptor unit.

### 3.2 Common features in donor–acceptor stacking

The relative arrangement between adjacent BTBT and TCNQ along the alternating stacking axis is quite similar in all 16 DA compounds. Fig. 4 presents the intermolecular arrangements for a pair of BTBT and TCNQ in five DA compounds, viewed along the axis perpendicular to the molecular plane. The stacking arrangements show the following common features: the sulphur atoms of BTBT, shown by blue-filled circles, are placed in the vacant space of TCNQ; and the outer carbon–carbon double bonds of TCNQ are located near the centre of the benzene or thiophene rings of BTBT. The former feature is associated with the van der Waals radius of sulphur being larger than that of carbon. It seems that the intermolecular interaction energy between the planar  $\pi$ -electron cores mainly determines the crystal structures, and the cores are arranged to decrease steric hindrance. Using intermolecular interaction calculations, we confirmed that such a relative arrangement is the most energetically stable, as discussed in the subsequent section.

Another common unique feature is that the direction of the alkyl chains forms a large angle (73.6°) with the long axis of the BTBT cores in the DA compound crystals with a bend at the root position. This angle is much larger than that of the single-component alkylated BTBT crystals (27.6° for *mono*-C<sub>9</sub>-BTBT). This large angle is formed by the gauche conformation of the carbon–carbon bonds closest to the BTBT cores (Supplementary Table S2 and Fig. S3). The alkyl chains were most probably forced to bend and fill spaces between the alkyl chains caused by the alternating acceptor units. Note that such a large angle between the alkyl chains and BTBT core is not formed in the interdigitated case of alkyl chains, as shown in Fig. 3 (other 1 and other 2). Notably, alkyl chains adopt an all-trans conformation in single-component alkylated BTBT crystals. We consider that such an energetically unstable conformation in the case of isolated molecules



**Fig. 5** (a) Coordinates of BTBT and TCNQ core skeletons for the calculation of the intermolecular interaction energy with a fixed intermolecular distance. The origin of the  $x$  axis is set at the actual structure. (b) Profiles of total interaction and respective contributions by dispersion, electrostatic, induction, and short-range orbit–orbit interaction.

could only be achieved in molecular compounds by the strong core–core interaction between the donor and acceptor units.

### 3.3 Origin of attractive forces in the DA compound

The common features observed for the donor–acceptor arrangements clearly indicate that strong and directional attractive forces exist between the  $\pi$ -electron cores of BTBT and TCNQ. To investigate the origin of the attraction between BTBT and TCNQ, we evaluated the intermolecular interaction energies and analysed the contributions of the electrostatic, induction, dispersion, and short-range orbit–orbit interactions. The intermolecular interaction energies were calculated with varying positions of TCNQ parallel to the molecular long axis ( $x$  axis) with a fixed interplanar distance from the BTBT molecule. The geometry of BTBT–TCNQ used for the calculations was obtained from the crystal structure data. Here, we set the origin of the  $x$  axis at the point of the actual donor–acceptor geometry in the crystals, as seen in Fig. 5a. It should be noted that a plot of total intermolecular interaction energy does not correspond to the potential energy surface associated with the horizontal displacement, as the interplanar distance was fixed in the calculations. The optimization of vertical displacement at each position is necessary to obtain potential energy surface. The calculations of fixed interplanar distance geometries were carried out to confirm which interactions play important roles in

DA compound		Space group	<i>a</i> (Å)	<i>b</i> (Å)	<i>c</i> (Å)	$\alpha$ (°)	$\beta$ (°)	$\gamma$ (°)	Stacking Structure
Donor	Acceptor								
	F0	$P2_1/c$	7.2227(3)	7.5676(2)	32.3247(12)	90	92.185(3)	90	Zigzag
DTT	F1	$P2_1/c$	7.1816(4)	7.5584(5)	33.058(3)	90	93.342(7)	90	Zigzag
	F2	$P2_1/c$	7.1277(3)	7.6492(3)	33.4443(13)	90	94.224(3)	90	Zigzag
	F0	$P\bar{1}$	7.6901(2)	7.9278(2)	8.0205(3)	79.566(3)	74.072(3)	80.581(2)	Alternating
BDT	F2	$P2_1/c$	7.4700(5)	6.8609(4)	18.4407(11)	90	98.585(6)	90	Alternating
	F4	$P2_1/c$	8.1770(3)	6.34763(18)	18.4338(5)	90	96.104(3)	90	Alternating

**Table 2** Unit cell parameters for (DTT)(F<sub>m</sub>)TCNQ and (BDT)(F<sub>m</sub>)TCNQ compounds.

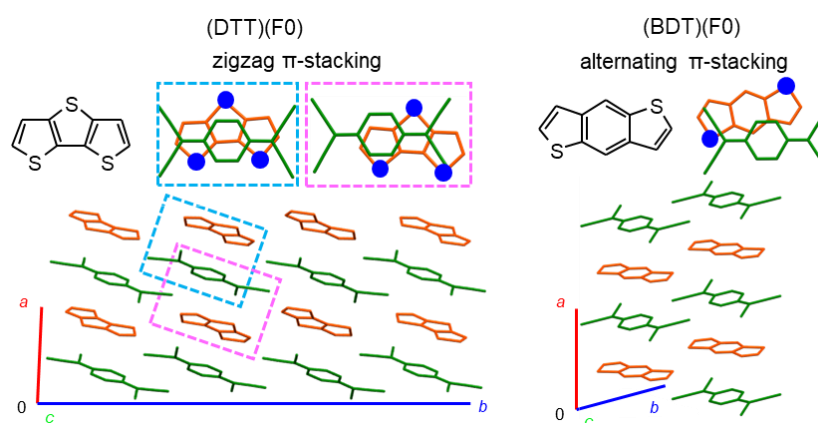


**Fig. 6** Crystal structures of the compounds with donor units other than the BTBT core skeleton. Donor and acceptor units are colored orange and green, respectively.

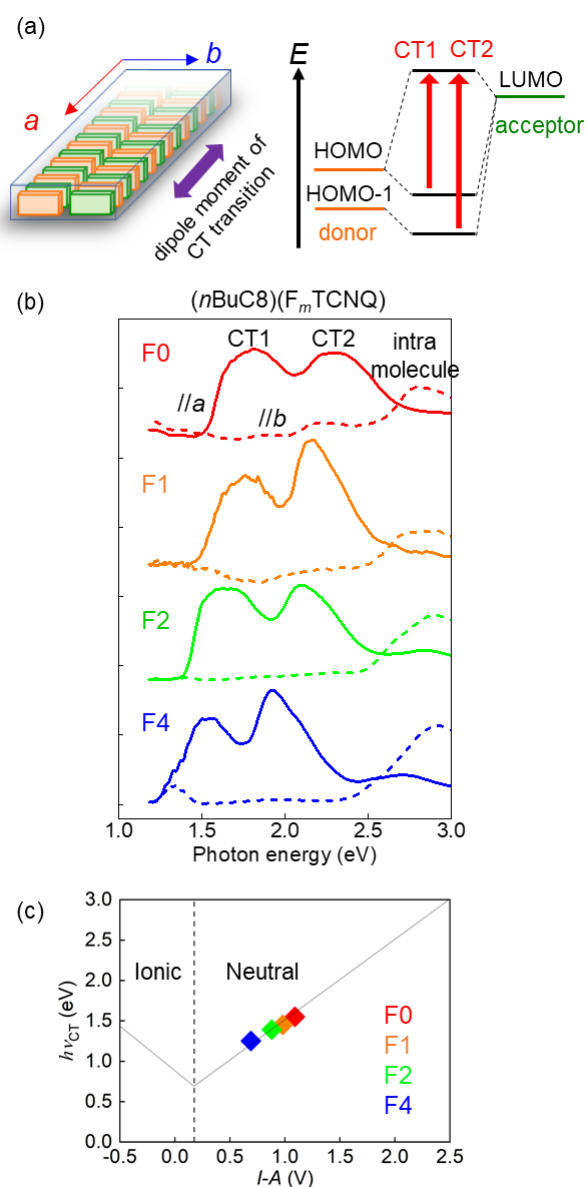
determining the arrangement of donor–acceptor molecules in crystals.

Fig. 5b presents a plot of the cross-sectional values along the *x*-axis for the total intermolecular interaction energy and respective contributions of the electrostatic, induction, dispersion, and short-range orbit–orbit interactions. The total intermolecular interaction energy is minimized at the origin, which is consistent with the crystal structures obtained from the experiments. The dispersion interaction dominated the attractive interaction, while the electrostatic and induction interactions were relatively smaller. The electrostatic interactions are attractive at the origin, as the negative charges of BTBT and the positive charges of TCNQ have close contact at the origin, as presented in Supplementary Fig. S4. The position dependence of the dispersion interactions is weak, if the interplanar distance from the BTBT is fixed. The total interaction energy has a minimum at the origin, since the repulsive short-range (orbit–orbit) interaction is weak at the origin. The weak repulsive short-range (orbit–orbit) interactions at the origin enables the short interplanar distance between BTBT and TCNQ, which enhances the attraction by the dispersion interactions. The position dependence of the dispersion and short-range (orbit–orbit) interactions shows that the magnitude of the repulsive short-range (orbit–orbit) interactions play important roles in determining the arrangements of donor and acceptor units in the crystals. The short-range (orbit–orbit)

interactions include the exchange-repulsion and CT interactions. The CT interactions may play important roles in determining the magnitude of the repulsive short-range interactions and control the arrangements of donor and acceptor units in the crystals, although the dispersion interactions are the major source of the attraction. Thus, we successfully quantitatively revealed the structural origin of the molecular-compound crystals using the dispersion corrected DFT calculations and the analysis of the contributions of each interaction. Our calculations clearly show that the dispersion interaction is the major source of the attraction in the crystal of donor–acceptor compound and the repulsive short-range (orbit–orbit) interactions play important roles in determining molecular arrangement in the crystal, although it was often claimed that the CT interactions were the main contributions to the attraction in donor–acceptor compound.

### 3.4 Case of dithieno[3,2-*b*:2',3'-*d*]thiophene and benzo[1,2-*b*:4,5-*b'*]dithiophene

We investigated the formation of molecular-compound crystals for two other thienoacene molecules as donor units: dithieno[3,2-*b*:2',3'-*d*]thiophene (DTT)<sup>51,52</sup> and benzo[1,2-*b*:4,5-*b'*]dithiophene (BDT)<sup>51</sup> (Fig. 6). We obtained crystals and successfully analysed the



**Fig. 7** (a) Schematics of the molecular arrangement and the energy levels of the molecular orbital in DA compounds. (b) Polarized absorption spectra in parallel to *a* and *b* axes for (nBuC8)(F<sub>m</sub>TCNQ) compounds. (c) Simple relationship between the CT energy and difference between the electrochemical oxidation-reduction potentials of the donor and acceptor, obtained by cyclic voltammetry measurements. *h* and *v* are the Planck constant and photon wavenumber, respectively.

crystal structures for six kinds of DA compounds, as listed in Table 2. The donor–acceptor stacking arrangement of DTT presents a similar tendency to that of (mTolC10)(F0), where the overlap between the donor and acceptor units is not equivalent along the stacks to form zigzag  $\pi$ -stacking; the intermolecular interaction energies in these arrangements are 0.74 and 0.56 eV, respectively. In sharp contrast, (BDT)(F<sub>m</sub>TCNQ) does not form a face-to-face arrangement, such as (BTBT derivatives)(F<sub>m</sub>TCNQ) compounds, although it has an alternating stacking structure. We consider that this unique feature is caused by the steric hindrance between the central benzene ring

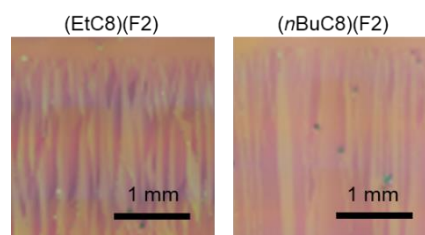


**Fig. 8** Crossed Nicols micrographs for the blade-coated compound films.

Compound		Electron mobility ( $\mu_{lin} / \mu_{sat}$ ) ( $\text{cm}^2 \text{V}^{-1} \text{s}^{-1}$ )	
Donor	Acceptor	Single crystal (BC)	Thin film (TC)
monoC12	F4	0.001 / 0.006	- / -
MeC8	F2	- / -	0.002 / $4 \times 10^{-4}$
	F0	- / -	0.04 / 0.003
EtC8	F2	$3 \times 10^{-4}$ / 0.003	0.02 / 0.004
	F4	$3 \times 10^{-4}$ / $3 \times 10^{-4}$	0.08 / 0.01
	F0	- / -	0.11 / 0.004
nBuC8	F2	$5 \times 10^{-4}$ / 0.01	0.007 / -
	F4	0.001 / 0.006	0.10 / 0.20
	F0	0.001 / 0.01	- / -
oTolC10	F2	$1 \times 10^{-4}$ / 0.001	- / -
	F4	- / -	0.10 / 0.16
mTolC10	F2	$2 \times 10^{-4}$ / 0.02	- / -
	F4	0.01 / 0.1	- / -
	F2	0.004 / 0.004	- / -
BDT	F4	$2 \times 10^{-4}$ / $6 \times 10^{-4}$	- / -

**Table 3** Field-effect mobilities for the DA compounds.

of BDT and the six-membered ring of TCNQ, where the two sulphur atoms of BDT may play a role. In this context, including thieno[3,2-*b*]thiophene in the donor unit to achieve face-to-face packing with TCNQ would be effective. These considerations are important for the design and development of molecular-compound OSCs with strong intermolecular interactions.

### 3.5 Optical and electrical properties

Optical absorption measurements were conducted to examine the excitation energies of the molecular compounds. The measurements were performed with irradiation of linearly polarized light parallel (*a* axis) and perpendicular (*b* axis) to the stacking axis along which the CT transition occurs (Fig. 7a). Fig. 7b shows the polarized absorption spectra of (nBuC8)(F<sub>m</sub>TCNQ). The two observed peaks, denoted as

CT1 and CT2, are both polarized parallel to the  $a$  axis and can be ascribed to the excitation from the HOMO and second HOMO levels, respectively, to the LUMO level. The intramolecular transition peak is visible at approximately 2.8 eV in parallel to the  $b$  axis.

We also investigated the dependence of the excitation energy on the change in the fluorine number in the  $F_m$ TCNQ. We found that the absorption edge shifted toward the lower energy side with increasing  $m$  in  $F_m$ TCNQ. This trend was observed for all (substituted BTBT)( $F_m$ TCNQ) compounds. This feature is associated with the simple relationship between the CT transition energy and the difference in the redox potentials of the donor and acceptor molecules, which is known as the V-shape diagram proposed by Torrance;<sup>27,54</sup> we confirmed that the molecular compounds agree well with this relationship (Fig. 7c). Here, we measured and used the cyclic voltammetry curves for 11 types of substituted BTBTs and four types of  $F_m$ TCNQ (Supplementary Fig. S5). The absorption spectra for (DTT)( $F_m$ TCNQ) and (BDT)(TCNQ) are shown in Supplementary Fig. S6.

Fig. 8 shows the crossed Nicols micrographs for the blade-coated films of (EtC8)(F2) and ( $n$ BuC8)(F2) fabricated on a parylene-coated substrate surface. The uniform area of the films was as large as a few square millimetres for these DA compounds. Typically, the use of unsymmetrically substituted BTBT tends to form large-area molecular-compound films, although such large-area uniformity is not always obtained for all DA compounds. We evaluated the field-effect mobility of the films by fabricating TFT device structures, in conjunction with the single-crystal FETs. A typical device characteristic is shown in Supplementary Fig. S7. All devices exhibited  $n$ -type characteristics, the results of which are summarized in Table 3. Owing to their large-area uniformity, these DA compounds have potential for application in printed electronic devices with stable  $n$ -type operation.

#### 4. Conclusions

We developed a family of  $n$ -type molecular DA compounds, mainly based on unsymmetrically substituted BTBTs and  $F_m$ TCNQ derivatives as the donor and acceptor units, respectively. Among them, 16 crystal structures were successfully analysed using single-crystal structure analyses. The crystal structures showed quite common intermolecular stacking arrangements between the planar donor and acceptor skeletons, irrespective of the type of substituent. These features clearly indicate that strong and directional intermolecular interactions occur between the planar  $\pi$ -electron cores of donors and acceptors. The dispersion corrected DFT calculations clearly show that the dispersion interaction is the major source of the attraction in the crystal of donor–acceptor compound and the repulsive short-range (orbit–orbit) interactions play important roles in determining molecular arrangement in the crystals, although it was often claimed that the CT interactions were the main contributions to the attraction in donor–acceptor compound. We believe that these findings will help search for and explore unique

combinations of molecules that afford superior semiconducting characteristics.

#### Author Contributions

SM and KO fabricated the DA compound crystals and contributed to all measurements. SI, THigashino, and MT synthesized the BTBT derivatives. SI, THigashino, RKondo, and RKumai analyzed the crystal structures. RO and ST calculated the intermolecular interactions. KN measured the thermal properties. THigashino and JT performed the cyclic voltammograms measurements. SA and THasegawa advised as to this investigation. SM and THasegawa wrote and edited this manuscript.

#### Conflicts of interest

There are no conflicts to declare.

#### Acknowledgements

This work was supported by JST CREST Grant Number JPMJCR1812 and JSPS KAKENHI grant numbers 19K15432, 19H02579, 20H05867, 21K05209, and 21H05234. Synchrotron radiation x-ray diffraction experiment were performed under the approval of the Photon Factory Program Advisory Committee (Proposal Number 2020S2-001).

#### References

- 1 D. Jérôme, *Chem. Rev.*, 2004, **104**, 5565.
- 2 M. Hiraoka, T. Hasegawa, T. Yamada, Y. Takahashi, S. Horiuchi and Y. Tokura, *Adv. Mater.*, 2007, **19**, 3248–3251.
- 3 H. Alves, A. S. Molinari, H. Xie and A. F. Morpurgo, *Nat. Mater.*, 2008, **7**, 574–580.
- 4 S. A. Odom, M. M. Caruso, A. D. Finke, A. M. Prokup, J. A. Ritchey, J. H. Leonard, S. R. White, N. R. Sottos and J. S. Moore, *Adv. Funct. Mater.*, 2010, **20**, 1721–1727.
- 5 K. P. Goetz, D. Vermeulen, M. E. Payne, C. Kloc, L. E. McNeil and O. D. Jurchescu, *J. Mater. Chem. C*, 2014, **2**, 3065–3076.
- 6 S. Horiuchi, R. Kumai, Y. Okimoto and Y. Tokura, *Chem. Phys.*, 2006, **325**, 78–91.
- 7 S. H. Lapidus, A. Naik, A. Wixtrom, N. E. Massa, V. T. Ta Phuoc, L. del Campo, S. Lebègue, J. G. Ángyán, T. Abdel-Fattah and S. Pagola, *Cryst. Growth Des.*, 2014, **14**, 91–100.
- 8 M. Masino, N. Castagnetti and A. Girlando, *Crystals*, 2017, **7**, 108.
- 9 H. Méndez, G. Heimel, A. Opitz, K. Sauer, P. Barkowski, M. Oehzelt, J. Soeda, T. Okamoto, J. Takeya, J. B. Arlin, J. Y. Balandier, Y. Geerts, N. Koch and I. Salzmann, *Angew. Chem. Int. Ed.*, 2013, **52**, 7751–7755.
- 10 J. Tsutsumi, S. Matsuoka, S. Inoue, H. Minemawari, T. Yamada and T. Hasegawa, *J. Mater. Chem. C*, 2015, **3**, 1976.
- 11 Y. Shibata, J. Tsutsumi, S. Matsuoka, K. Matsubara, Y. Yoshida, M. Chikamatsu and T. Hasegawa, *Appl. Phys. Lett.*, 2015, **106**, 143303.
- 12 K. P. Goetz, J. Tsutsumi, S. Pookpanratana, J. Chen, N. S. Corbin, R. K. Behera, V. Coropceanu, C. A. Richter, C. A. Hacker, T. Hasegawa, and O. D. Jurchescu, *Adv. Electron. Mater.*, 2016, **2**, 1600203.

- 13 R. R. Dasari, X. Wang, R. A. Wiscons, H. F. Haneef, A. Ashokan, Y. Zhang, M. S. Fonari, S. Barlow, V. Coropceanu, T. V. Timofeeva, O. D. Jurchescu, J.-L. Brédas, A. J. Matzger, and S. R. Marder, *Adv. Funct. Mater.*, 2019, **29**, 1904858.
- 14 Y. Shibata, J. Tsutsumi, S. Matsuoka, H. Minemawari, S. Arai, R. Kumai and T. Hasegawa, *Adv. Electron. Mater.*, 2017, **3**, 1700097.
- 15 H. Usta, A. Facchetti and T. J. Marks, *Acc. Chem. Res.*, 2011, **44**, 501–510.
- 16 H. Matsui, Y. Takeda and S. Tokito, *Org. Electron.*, 2019, **75**, 105432.
- 17 H. Minemawari, T. Yamada, H. Matsui, J. Tsutsumi, S. Haas, R. Chiba, R. Kumai and T. Hasegawa, *Nature*, 2011, **475**, 364–367.
- 18 Y. Yuan, G. Giri, A. L. Ayzner, A. P. Zoombelt, S. C. B. Mannsfeld, J. Chen, D. Nordlund, M. F. Toney, J. Huang and Z. Bao, *Nat. Commun.*, 2014, **5**, 3005.
- 19 H. Iino, T. Usui and J. Hanna, *Nat. Commun.*, 2015, **6**, 6828.
- 20 T. Hamai, S. Arai, H. Minemawari, S. Inoue, R. Kumai and T. Hasegawa, *Phys. Rev. Appl.*, 2017, **8**, 054011.
- 21 T. Hamai, S. Inoue, S. Arai, T. Hasegawa, *Phys. Rev. Materials*, 2020, **4**, 074601.
- 22 S. Inoue, H. Minemawari, J. Tsutsumi, M. Chikamatsu, T. Yamada, S. Horiuchi, M. Tanaka, R. Kumai, M. Yoneya and T. Hasegawa, *Chem. Mater.*, 2015, **27**, 3809–3812.
- 23 T. Higashino, M. Dogishi, Y. Kadoya, R. Sato, T. Kawamoto and T. Mori, *J. Mater. Chem. C*, 2016, **4**, 5981.
- 24 H. Minemawari, M. Tanaka, S. Tsuzuki, S. Inoue, T. Yamada, R. Kumai, Y. Shimoï and T. Hasegawa, *Chem. Mater.*, 2017, **29**, 1245–1254.
- 25 S. Inoue, K. Nikaido, T. Higashino, S. Arai, M. Tanaka, R. Kumai, S. Tsuzuki, S. Horiuchi, H. Sugiyama, Y. Segawa, K. Takaba, S. Maki-Yonekura, K. Yonekura and T. Hasegawa, *Chem. Mater.*, 2022, **34**, 72–83.
- 26 S. Inoue, T. Higashino, S. Arai, R. Kumai, H. Matsui, S. Tsuzuki, S. Horiuchi and T. Hasegawa, *Chem. Sci.*, 2020, **11**, 12493–12505.
- 27 J. B. Torrance, NATO ASI Series, ed. by D. Jerome, L. G. Caron, Plenum Press, New York, London, 1987, pp. 113–133.
- 28 R. G. Kepler, P. E. Bierstedt and R. E. Merrifield, *Phys. Rev. Lett.*, 1960, **5**, 503–504.
- 29 D. S. Acker, R. J. Harder, W. R. Hertler, W. Mahler, L. R. Melby, R. E. Benson and W. E. Mochel, *J. Am. Chem. Soc.*, 1960, **82**, 6408.
- 30 R. C. Wheland and E. L. Martin, *J. Org. Chem.*, 1975, **40**, 3101–3109.
- 31 CrysAlisPro, Data Collection and Processing Software, Rigaku Corp., 2015.
- 32 L. J. Bourhis, O. V. Dolomanov, R. J. Gildea, J. A. K. Howard, H. Puschmann, *Acta Crystallogr. A Found. Adv.*, 2015, **71**, 59, Sect. A.
- 33 G. M. Sheldrick, *Acta Crystallogr. C Struct. Chem.*, 2015, **71**, 3–8.
- 34 M. J. Frisch, G. W. Trucks, H. B. Schlegel, G. E. Scuseria, M. A. Robb, J. R. Cheeseman, G. Scalmani, V. Barone, G. A. Petersson, H. Nakatsuji, X. Li, M. Caricato, A. V. Marenich, J. Bloino, B. G. Janesko, R. Gomperts, B. Mennucci, H. P. Hratchian, J. V. Ortiz, A. F. Izmaylov, J. L. Sonnenberg, D. Williams-Young, F. Ding, F. Lipparini, F. Egidi, J. Goings, B. Peng, A. Petrone, T. Henderson, D. Ranasinghe, V. G. Zakrzewski, J. Gao, N. Rega, G. Zheng, W. Liang, M. Hada, M. Ehara, K. Toyota, R. Fukuda, J. Hasegawa, M. Ishida, T. Nakajima, Y. Honda, O. Kitao, H. Nakai, T. Vreven, K. Throssell, J. A. Montgomery, J. E. Peralta Jr, F. Ogliaro, M. J. Bearpark, J. J. Heyd, E. N. Brothers, K. N. Kudin, V. N. Staroverov, T. A. Keith, R. Kobayashi, J. Normand, K. Raghavachari, A. P. Rendell, J. C. Burant, S. S. Iyengar, J. Tomasi, M. Cossi, J. M. Millam, M. Klene, C. Adamo, R. Cammi, J.W. Ochterski, R. L. Martin, K. Morokuma, O. Farkas, J. B. Foresman and D. J. Fox, *Gaussian16*, Revision, C. 01, Gaussian Incorp., Wallingford, Connecticut, 2016.
- 35 A. D. Becke, *J. Chem. Phys.*, 1993, **98**, 5648–5652.
- 36 S. Grimme, J. Antony, S. Ehrlich and H. Krieg, *J. Chem. Phys.*, 2010, **132**, 154104.
- 37 B. J. Ransil, *J. Chem. Phys.*, 1961, **34**, 2109–2118.
- 38 S. F. Boys and F. Bernardi, *Mol. Phys.*, 1970, **19**, 553–566.
- 39 S. Tsuzuki and T. Uchimaru, *Phys. Chem. Chem. Phys.*, 2020, **22**, 22508–22519.
- 40 J. A. Pople, M. Head-Gordon, and K. Raghavachari, *J. Chem. Phys.*, 1987, **87**, 5968–5975.
- 41 G. E. Scuseria, and H. F. Schaefer, *J. Chem. Phys.*, 1989, **90**, 3700–3703.
- 42 A. J. Stone, A. Dullweber, M. P. Hodges, P. L. A. Popelier and D. J. Wales, *Orient: A Program for Studying Interactions between Molecules Version 3.2*, University of Cambridge, 1995.
- 43 A. J. Stone, M. Alderton, *Mol. Phys.*, 1985, **56**, 1047–1064.
- 44 A. J. Stone, *The Theory of Intermolecular Forces*, 2nd ed., Oxford University Press, Oxford, 2013.
- 45 A. J. Stone, *J. Chem. Theory Comput.*, 2005, **1**, 1128–1132.
- 46 A. J. Stone, *Mol. Phys.*, 1985, **56**, 1065.
- 47 P. T. van Duijnen and M. Swart, *J. Phys. Chem. A*, 1998, **102**, 2399–2407.
- 48 Z.-Y. Yang, H.-M. Zhang, C.-J. Yan, S.-S. Li, H.-J. Yan, W.-G. Song and L.-J. Wan, *Proc. Natl. Acad. Sci.*, 2007, **104**, 3707–3712.
- 49 R. J. Kline, D. M. DeLongchamp, D. A. Fischer, E. K. Lin, L. J. Richter, M. L. Chabinc, M. F. Toney, M. Heeney and I. McCulloch, *Macromolecules*, 2007, **40**, 7960–7965.
- 50 N. Nishitani, T. Hirose and K. Matsuda, *Chem. Lett.*, 2019, **48**, 253–256.
- 51 R. Castañeda, V. N. Khrustalev, A. Fonari, J.-L. Bredas, Y. A. Getmanenko and T. V. Timofeeva, *J. Mol. Struct.*, 2015, **1100**, 506–512.
- 52 L. Jones, C. M. Pask, A. Kazlaucinas, M. Gulcur and L. Lin, *ChemistrySelect*, 2017, **2**, 5958–5964.
- 53 K. Takimiya, Y. Konda, H. Ebata, N. Niihara and T. Otsubo, *J. Org. Chem.*, 2005, **70**, 10569–10571.
- 54 J. B. Torrance, *Mol. Cryst. Liq. Cryst.*, 1985, **126**, 55–67.